M&C 2017 - International Conference on Mathematics & Computational Methods Applied to Nuclear Science & Engineering, Jeju, Korea, April 16-20, 2017, on USB (2017)

A Review of the Upstream Corner Balance Spatial Discretization

Peter G. Maginot,* Paul F. Nowak,* Marvin L. Adams†

*Lawrence Livermore National Laboratory, 7000 East Avenue, Livermore, CA 94551
†Department of Nuclear Engineering, Texas A&M University, 3133 TAMU, College Station, TX 77843
maginot1@llnl.gov, pnowak2@llnl.gov, mladams@tamu.edu*

Abstract - *In this work, we document and study two variants of upstream corner balance (UCB) spatial discretizations for the linear Boltzmann equation. The first variant of UCB was published in 1997 by Adams. The second variant corrects a flaw, discovered in 2005, inherent in the 1997 variant. The second (2005) variant has not previously been published. Computational results are presented to: demonstrate the equivalence of the two UCB methods in slab geometry, verify that the second variant of UCB corrects the multi-dimensional flaw of the original UCB, and explore the accuracy of UCB relative to the more widely known and used bilinear discontinuous finite element spatial discretizations. Each UCB method studied here performs well in some limits but poorly in other limits.*

I. INTRODUCTION

The original upstream corner balance (UCB) spatial discretization was published by Adams in [1]. We refer to this variant of UCB as UCB97. In 2005, a flaw was found with UCB97 for problems in multiple spatial dimensions given unequal incident angular fluxes on adjacent faces of a given zone. (In this paper, "zone" and "spatial cell" are synonymous.) To correct this flaw, a new variant of UCB was derived which we refer to as UCB05. To the best collective knowledge of this paper's authors and our collaborators [2] who have also studied UCB, UCB05 has never been documented within the radiation transport literature.

In this work, we more clearly re-state the UCB97 spatial discretization originally given in [1]. We demonstrate how UCB05 can be derived from UCB97 and show the equivalence of UCB97 to UCB05 in slab-geometry problems. The ray-propagation problem of Mathews [3] is then used to demonstrate the instability of UCB97 and the stability of UCB05. Finally, the UCB05 and UCB97 spatial discretizations are studied and compared to an unlumped bilinear discontinuous finite element discretization (UBLD) and a fully lumped bilinear discontinuous finite element (FLBLD) discretization for the ray-propagation problem and problems devised using the method of manufactured solutions (MMS) [4]. This study considers two different interpretations of the UCB unknowns—that they are centered at vertices or centered in subcell volumes—and illustrates that the interpretation one chooses can significantly affect the accuracy one observes.

II. DERIVATIONS

1. Upstream Corner Balance Methods

UCB spatial discretizations are most easily defined for the steady-state, mono-energetic, mono-directional linear Boltzmann equation,

$$\vec{\Omega} \cdot \vec{\nabla}\psi + \sigma_t \psi = Q\,. \tag{1}$$

In Eq. (1), $\vec{\Omega}$ is particle direction, $\psi(\vec{x}, \vec{\Omega})$ is the angular flux, $\sigma_t(\vec{x})$ is the total interaction cross section, $Q(\vec{x}, \vec{\Omega})$ is the directionally dependent total source (which may include scattering, fission, emission, etc., in addition to the fixed source), and $\vec{x}$ is position.

All corner balance methods, UCB included, are defined by enforcing particle balance within each individual "corner," which is a sub-cell of a spatial mesh cell (zone). A corner is a half-cell in slab geometry, a quadrilateral in 2-D, and a polyhedron in 3-D. Corner balance methods differ in their approximations for how exiting-surface-averaged fluxes relate to volume-averaged and incident-surface-averaged fluxes. In this paper, we examine UCB schemes for slab cells and 2-D polygons, deferring the more complicated 3-D discussion to a later communication. As shown in Fig. 1, the quadrilateral corner "c" of the larger arbitrary-polygon spatial mesh zone "z" has a total of four faces: two zone-interior faces shared with corners c_- and c_+, respectively, and two zone-surface faces shared with corners of adjacent zones. See [5] for further clarification on the relationship between zones and their corners.

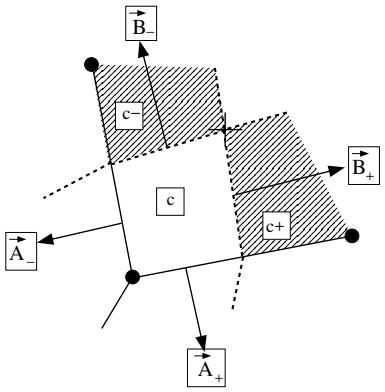

Fig. 1. A portion of a spatial zone (cell) showing the quadrilateral corner c, its surface area vectors, and its zone-interior neighboring corners ($c+$ and $c-$). A corner in 2-D is a quadrilateral defined by a zone vertex, the midpoints of the two connected edges, and the zone center point. The N corners in a polygonal zone with N vertices fill the zone and do not overlap.

All corner balance schemes impose particle conservation within each corner:

$$\vec{\Omega}\cdot\left[\vec{A}_{-}\psi_{z-1/2}+\vec{A}_{+}\psi_{z+1/2}+\vec{B}_{+}\psi_{c+1/2}+\vec{B}_{-}\psi_{c-1/2}\right] + V_c\sigma_{t,c}\psi_c = V_c Q_c\,. \quad (2)$$

In Eq. (2), $\vec{A}_{\pm}$ and $\vec{B}_{\pm}$ are the area face normals, the area of the face multiplied by the outward direct normal of that face, as shown in Fig. 1; V_c is the volume of corner c (= area in 2D); and $\sigma_{t,c}$ is the corner-averaged total cross section. In this paper we consider only problems with zone-wise constant cross sections and henceforth omit the c subscript on σ_t. In Eq. (2), there are five angular flux quantities,

1. ψ_c, the volumetric average angular flux within corner c,
2. $\psi_{z\pm1/2}$, the average angular fluxes along the zone interfaces of corner c, and
3. $\psi_{c\pm1/2}$, the average angular fluxes along the zone-interior interfaces of corner c.

A schematic of the locations of the interface fluxes and the corner-average fluxes is given in Fig. 2.

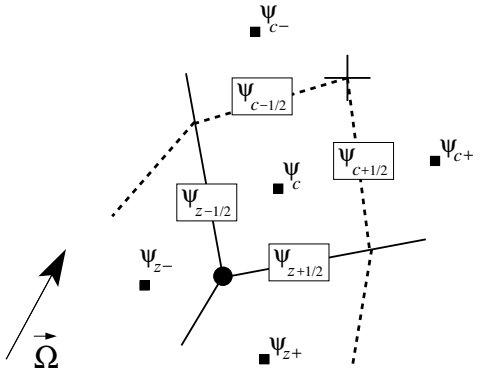

Fig. 2. Location of interface fluxes, $\psi_{c\pm1/2}$ and $\psi_{z\pm1/2}$, relative to the corner average fluxes, ψ_c and $\psi_{c\pm}$ of zone z. Solid black lines denote zone boundaries, and dashed lines indicate corner boundaries within a zone. The crosshairs denote the zone center.

Though all corner balance schemes enforce the same equation [Eq. (2)], each corner balance scheme has unique accuracy, performance, and other characteristics based on how that scheme defines the various interface fluxes. Both UCB97 and UCB05 use upwinding at zone interfaces, defining

$$\psi_{z\pm1/2} = \begin{cases} \psi_c & \vec{\Omega}\cdot\vec{A}_{\pm} > 0 \\ \psi_{z\pm} & \vec{\Omega}\cdot\vec{A}_{\pm} < 0 \end{cases}\,. \quad (3)$$

Here the $\psi_{z\pm}$ quantities are given from neighboring cells or boundary conditions. The performance of UCB depends on its definition of the zone-interior inter-corner interface fluxes. The UCB interface flux definitions allow for

1. solving corner by corner for all corner-average and corner-exiting fluxes of a given zone without explicitly building and solving a system of linear algebraic equations for the entire zone,
2. reasonable accuracy in the thick diffusion limit [6, 7, 8], and
3. minimizing 1-D truncation error [1].

The first point is the origin of the "upstream" designation for UCB: for a given direction $\vec{\Omega}$, the "upstreaming" nature of UCB defines a system of linear equations that is strictly lower triangular and can be solved corner by corner within each zone.

All UCB schemes define the inter-corner interface flux from the point of view of the "upstream" corner—the corner for which the inter-corner interface is an outflow face. Using Fig. 2 as an example where $\vec{\Omega}\cdot\vec{B}_{+} > 0$, UCB97 defines the outgoing flux $\psi_{c+1/2}$ as:

$$\psi_{c+1/2} = \psi_c + \frac{Q_{c+} - Q_c}{2\sigma_t} + f(\tau_{c+1/2})[\psi_c - \psi_{z-1/2}]\,, \quad (4)$$

where $\tau_{c+/1/2}$ is an effective optical depth of corner c with respect to the c+1/2 face, for the direction ($\vec{\Omega}$) for which the equation is being solved:

$$\tau_{c\pm1/2} = \sigma_t\frac{V_c}{\vec{\Omega}\cdot\vec{B}_{\pm}}\,, \quad \vec{\Omega}\cdot\vec{B}_{\pm} > 0\,, \quad (5)$$

where V is the volume of the corner, $\vec{B}$ is the outward directed area normal, and σ_t and $\vec{\Omega}$ are as defined previously. From [1], the $f(\tau)$ of Eq. (4) is defined as

$$f(\tau) = \frac{3+4\tau+4\alpha\tau^2}{2\tau+2\tau^2+4\tau^3}\,. \quad (6)$$

(Our notation differs from that of [1]. Our α is the "α_0" from [1], and our $f(\tau)$ equals $\alpha(\tau)/\tau$ from [1].) The $f(\tau)$ form was chosen because it leads to satisfactory results in the thick diffusion limit and provides small truncation error in the outflow angular flux in a slab-geometry source-free pure absorber. The α constant in Eq. (6) is a free parameter. As originally detailed in [1], this constant is set to 0.455 in UCB97 to maximize accuracy in the presence of unresolved boundary layers in the thick diffusion limit.

2. A Lurking Problem

UCB97 can be used without apparent issue in a variety of practical problems. However, the method contains a serious flaw that leads to unacceptable performance in some problems. Observe that in the limit as $\tau \to 0$, from Eq. (6) $f(\tau) \to \frac{3}{2\tau}$, which becomes unbounded as the optical depth, τ, approaches zero. This flaw is hidden if the term multiplied by $f(\tau)$, $\psi_c - \psi_{z-1/2}$, approaches zero at a rate greater than or equal to the rate $f(\tau)$ goes to infinity. In slab geometry UCB97 is a stable, well behaved discretization, because (as we show below) the product $f(\tau)[\psi_c - \psi_{z-1/2}]$ is well behaved as $\tau \to 0$. In multi-dimensional problems with relatively smooth solutions this is also the case, but in some multi-dimensional problems $\psi_c - \psi_{z\pm1/2}$ does not go to zero quickly enough to keep the product well-behaved.

We now demonstrate that in slab geometry,

$$\lim_{\tau\to 0}\left\{f(\tau)\left[\psi_c-\psi_{z-1/2}\right]\right\}=0\,. \tag{7}$$

In slab geometry, the corner c balance equation is:

$$\psi_{c+1/2}-\psi_{z-1/2}+\tau\psi_c=\tau\frac{Q_c}{\sigma_t}\,, \tag{8}$$

where he have defined $\tau=\sigma_t\Delta x_c/\mu$, Δx_c is the width of corners c and c_+, and μ is the cosine of $\vec{\Omega}$ with respect to the $x-$axis. This equation and Eq. (4) are the two equations that determine ψ_c and $\psi_{c+1/2}$ when $\psi_{z-1/2}$ is incoming. Algebraic manipulation of these two equations leads to:

$$f(\tau)\left[\psi_c-\psi_{z-1/2}\right]=\frac{f(\tau)}{1+\tau+f(\tau)}\left[\frac{3Q_c-Q_{c+}}{2\sigma_t}-\tau\psi_{z-1/2}\right], \tag{9}$$

It is easy to see that

$$\lim_{\tau\to 0}\left\{f(\tau)\left[\psi_c-\psi_{z-1/2}\right]\right\}=\frac{3Q_c-Q_{c+}}{2\sigma_t}\,, \tag{10}$$

verifying that $f(\tau)[\psi_c-\psi_{z-1/2}]$ is a bounded quantity *in slab geometry*.

3. UCB05 from UCB97

Equation (9) can be thought of as a UCB97 slab-geometry identity. Using Eq. (9), Eq. (4) can alternatively be expressed as

$$\psi_{c+1/2}=\psi_c+\frac{Q_{c+}-Q_c}{2\sigma_t}+\frac{f(\tau)}{1+\tau+f(\tau)}\left[\frac{3Q_c-Q_{c+}}{2\sigma_t}-\tau\psi_{z-1/2}\right]. \tag{11}$$

Defining $\psi_{c+1/2}$ as in Eq. (11) is equivalent to defining it as in Eq. (4), *in slab geometry*. However, Eq. (11) differs from Eq. (4) in that it does contain the product of a function that $\to\infty$ times a function that $\to 0$ in the limit of $\tau\to 0$.

Equation (11) is the UCB05 inter-corner interface flux definition. It produces the same solution as UCB97 in slab geometry but different solutions in multi-dimensional geometries in general. We rewrite this UCB05 equation as

$$\psi_{c+1/2}=\psi_c+\frac{Q_{c+}-Q_c}{2\sigma_t}\left[1-g(\tau)\right]+g(\tau)\left[\frac{Q_c}{\sigma_t}-\tau\psi_{z-1/2}\right], \tag{12}$$

where

$$g(\tau)\equiv\frac{\tau f(\tau)}{\tau f(\tau)+\tau+\tau^2}\,. \tag{13}$$

The g and $(1-g)$ functions are well-behaved, with g monotonically decreasing from 1 at $\tau=0$ to 0 as $\tau\to\infty$. The product $\tau g(\tau)$ also decreases to 0 as $\tau\to\infty$. Thus, the coefficients of the driving terms (sources and incident fluxes) in the UCB05 equation are all well-behaved.

Since Eq. (12) is derived from UCB97 in slab geometry, UCB05 will yield identical results as UCB97 in slab geometry. However, since all terms in Eq. (12) are finite as τ approaches zero, we expect UCB05 to remain stable in multi-dimensional geometry in cases where UCB97 becomes unstable.

III. COMPUTATIONAL RESULTS

1. Slab Geometry Equivalence

In Fig. 3, we plot the inflow-normalized corner-c average flux, $\psi_c/\psi_{z-1/2}$, for a source-free, purely absorbing medium as a function of corner effective optical thickness, τ. Figure 3 demonstrates that UCB05 is equivalent to UCB97 in slab geometry, and shows that UCB97 yields strictly positive solutions in a source-free pure absorber.

We plot the UCB97 and UCB05 corner-c normalized solutions, $\psi_c/\left(\frac{Q_c}{\sigma_t}\right)$, for a source-driven problem with vacuum boundary conditions for the three different ratios of source skew, Q_{c+}/Q_c, as a function of τ in Fig. 4. Again, Fig. 4 confirms that UCB05 is equivalent to UCB97 in slab geometry. Additionally, Fig. 4 shows an interesting artifact of UCB and discontinuous finite element spatial discretizations of the linear Boltzmann equation: strong sources, in particular geometrically skewed source distributions that are largest near cell outflows, can result in negative angular flux solutions near zone inflows, despite yielding positive outflow angular fluxes. The magnitude of the negativity in Fig. 4 is magnified by our choice of normalization. If instead of plotting $\psi_c/\frac{Q_c}{\sigma_t}$, we had plotted $\psi_c/\frac{Q_{c+}}{\sigma_t}$, the negativity would be much smaller, as $Q_{c+}/Q_c=10$ for the UCB solutions that yielded negative ψ_c. It is important to recognize that although ψ_c can be <0 for corners adjacent to "inflow" surfaces, the zone-averaged and zone-exiting fluxes in these test problems are all >0.

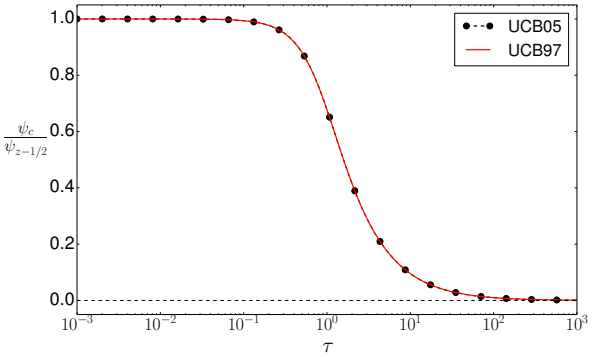

Fig. 3. UCB97 and UCB05 normalized value of ψ_c for a source-free, pure absorber.

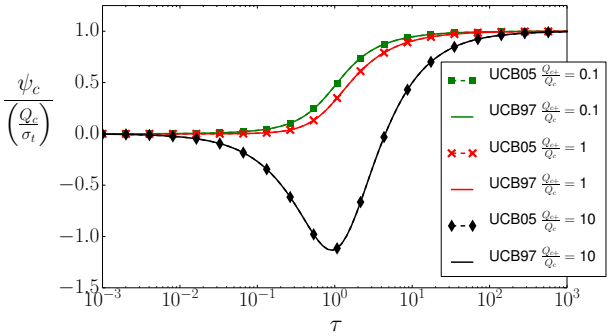

Fig. 4. UCB97 and UCB05 normalized solutions for a source driven problem.

2. Ray Propagation Problem

The instability of UCB97 arises when incident angular fluxes on adjacent zone-surfaces in a given corner do not become equal as $\tau \to 0$. The effects are exacerbated by optically thin zones and zones with large aspect ratios. To demonstrate this instability, we consider the ray-propagation problem of Mathews [3]. As described in [3], the problem consists of a $(x, y) \in [0, 25] \times [0, 25]$ homogenous, source free pure absorbing medium, with $\sigma_t = 1$. Vacuum boundary conditions exist on all faces for all directions, except for angular flux in the direction of $\mu = 0.3500212$, $\eta = 0.8688903$ incident along the bottom edge of the domain for $x \in [0, 0.5]$.

In Fig. 5, we compare the normalized angular flux solution, $\widehat{\psi}(x)$,

$$\widehat{\psi}(x) = \frac{\psi_{num}(x, 25)}{\int_0^{25} \psi_{num}(x, 25)\, dx}, \tag{14}$$

of UCB97, UCB05, UBLD, and FLBLD, to the analytic solution for the nominal case of uniform zones with $\Delta x = \Delta y = 0.5$. As noted by Mathews, nearly all spatial discretizations will broaden the incident beam of radiation and possibly translate the beam position artificially, phenomena that every method in Fig. 5 exhibit.

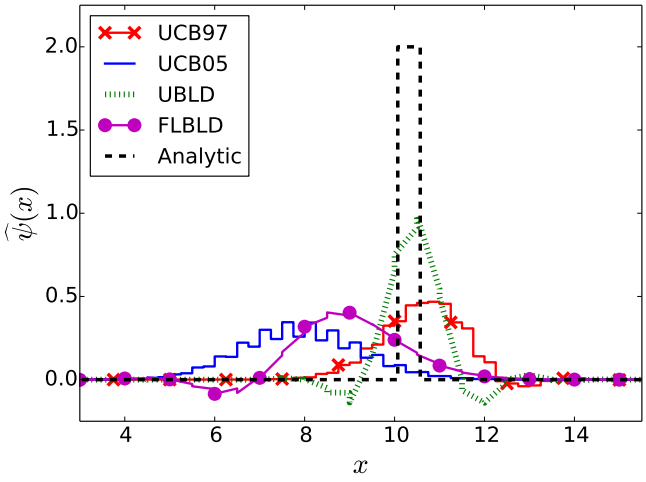

Fig. 5. Normalized angular flux, $\widehat{\psi}(x)$, at $y = 25$, with $\Delta x = \Delta y = 0.5$ for Mathews' ray propagation test problem.

The original motivation for the development of 2-D "simple" corner balance (SCB) was to obtain FLBLD-like solutions on polygonal cells with more than four vertices [1]. The original motivation for UCB was to obtain similar solutions without building and inverting matrices for each cell, and to improve on those solutions if possible [1]. We see from Fig. 5 that UCB97 is arguably better than FLBLD and comparable to UBLD, for this problem, and UCB05 is comparable to FLBLD.

In Fig. 6, we plot the UCB97 solution at different mesh refinements, with $\Delta y = 2\Delta x$. Though some oscillation near the expected beam location could be tolerated, UCB97 is unstable in this regime, with oscillations that grow with refinement and with distance from the beam. This is a direct result of the

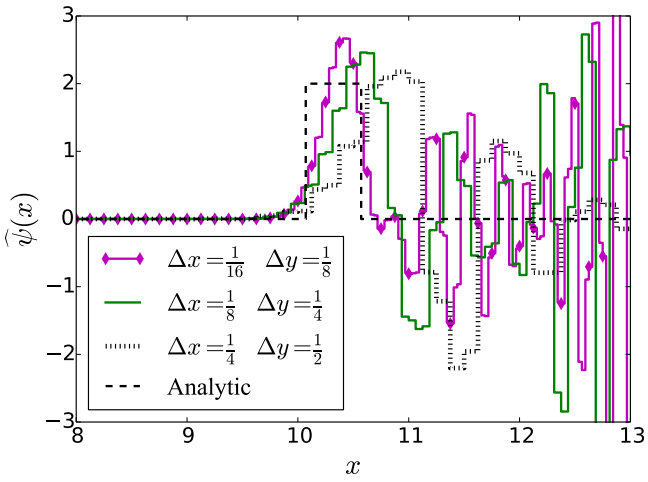

Fig. 6. $\widehat{\psi}(x)$ for UCB97 at $y = 25$, with $2\Delta x = \Delta y = 0.5$ for the ray propagation problem at different levels of mesh refinement.

"flaw" identified above.
For comparison, consider the UBLD and UCB05 solutions, given in Fig. 7 and Fig. 8, respectively. The UBLD solution is clearly more accurate than UCB05, which exhibits significant spreading and shifting of the beam. However, UCB05:

- remains stable,
- yields non-negative solutions for this test problem,
- becomes more accurate with mesh refinement, and
- can be applied to polygonal zones, whereas UBLD and FLBLD cannot.

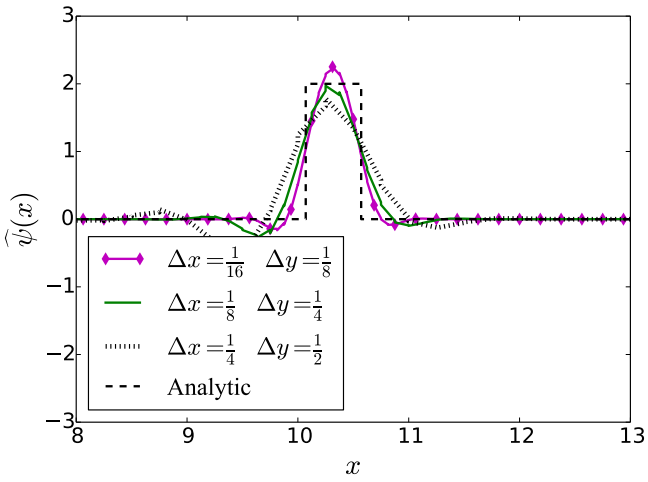

Fig. 7. $\widehat{\psi}(x)$ for UBLD at $y = 25$, with $2\Delta x = \Delta y = 0.5$ for the ray propagation problem at different levels of mesh refinement.

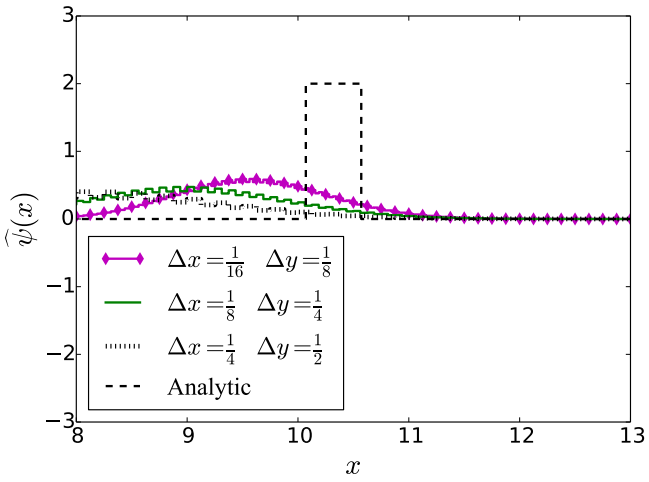

Fig. 8. $\widehat{\psi}(x)$ for UCB05 at $y = 25$, with $2\Delta x = \Delta y = 0.5$ for the ray propagation problem at different levels of mesh refinement.

For radiative transfer applications, UBLD is more prone to negativities than is FLBLD. As such, and given the original goals of UCB development, a fair comparison is the accuracy of UCB05 to the accuracy of FLBLD. Returning to the case of uniform zones, we compare the normalized angular flux outflow from the top of the domain for FLBLD in Fig. 9 to that of UCB05 given in Fig. 10 for various mesh refinements. The FLBLD scheme broadens and translates the beam less than UCB05 for an equal number of unknowns. That is, UCB05 is more "diffusive" than FLBLD for this problem. The FLBLD solution contains negativities that, while mitigated with mesh refinement, cannot be eliminated entirely, whereas the UCB05 outflow is strictly positive.

In summary, for beam propagation UCB97 can produce unacceptable oscillations, whereas UCB05 produces solutions that resist negativities and oscillations but exhibit more numerical diffusion than FLBLD or UBLD.

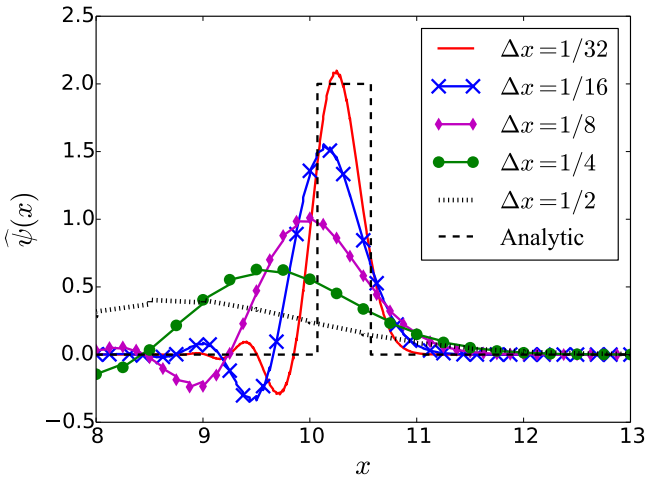

Fig. 9. $\widehat{\psi}(x)$ for FLBLD at $y = 25$, with $\Delta x = \Delta y$ at varying levels of mesh refinement.

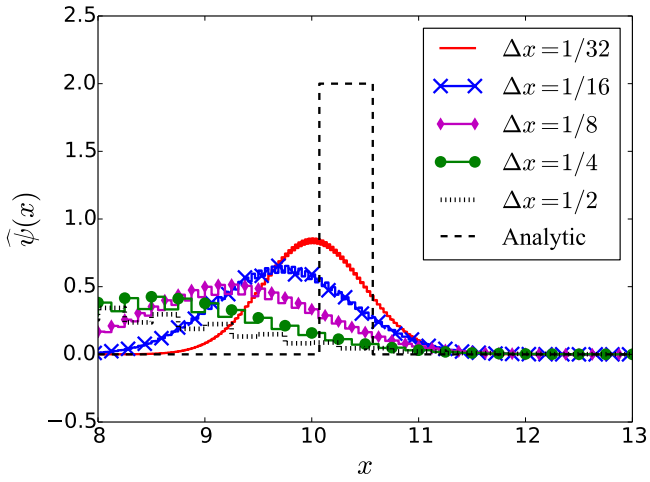

Fig. 10. $\widehat{\psi}(x)$ for UCB05 at $y = 25$, with $\Delta x = \Delta y$ at varying levels of mesh refinement.

3. Bilinear MMS Comparison

Here we consider a simple test problem with a bilinear analytic solution and explore how well the UCB methods achieve their goal of approximating such a solution. We use the Method of Manufactured Solutions (MMS) to define an angular flux solution of the form $\psi(x, y) = 1 + x(3 - y)$, with $x \in [0, 1]$, $y \in [0, 1]$, $\mu = 0.3500212$ and $\eta = 0.8688903$, $\sigma_t = 1$, and no scattering within the medium, on a single-zone mesh, $\Delta x = \Delta y = 1$. Our error metric assesses the difference between the numerical and analytic zone-averaged fluxes. This is the one-zone limit of the following more general metric, which we will use below in more complicated MMS problems:

$$E_A = \sqrt{\sum_{z=1}^{N_z} \Delta x \Delta y \left(\psi_A - \widetilde{\psi}_A\right)_z^2}, \tag{15}$$

where $\psi_{A,z}$ and $\widetilde{\psi}_{A,z}$ are the exact and numerical zone-averaged angular fluxes, respectively, within zone "z."

Before we apply the numerical methods to the MMS test problem, a discussion of the UCB unknowns is in order. As noted by Adams, the FLBLD equations are identical to the simple corner balance (SCB) equations for rectangular zones with zone-wise constant cross section [7]. However, while the equations are identical, the unknowns in the respective systems of equations could be interpreted differently. The FLBLD unknowns are vertex values of a bilinear interpolatory function, whereas the SCB solution unknowns could be viewed as either those same vertex values or as average angular fluxes over the corner subcells of the zone. UCB unknowns also have these two plausible interpretations.

The relation between vertex and corner-averaged quantities is easy to find for bilinear functions. Consider Fig. 11, which depicts vertex and corner indices for a rectangular cell. Let $\hat{\psi}_j$ be the value at the j-th vertex and ψ_j be the value

averaged over the adjacent corner subcell. Then

$$\frac{1}{16}\begin{bmatrix}9 & 3 & 3 & 1\\ 3 & 9 & 1 & 3\\ 3 & 1 & 9 & 3\\ 1 & 3 & 3 & 9\end{bmatrix}\begin{bmatrix}\hat{\psi}_1\\ \hat{\psi}_2\\ \hat{\psi}_3\\ \hat{\psi}_4\end{bmatrix} = \begin{bmatrix}\psi_1\\ \psi_2\\ \psi_3\\ \psi_4\end{bmatrix}. \tag{16}$$

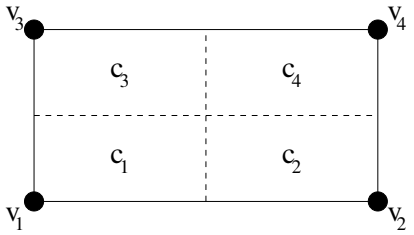

Fig. 11. Vertex and corner numbering pattern for rectangular cell.

The average of the four $\hat{\psi}_j$ quantities equals the average of the four ψ_j quantities. Thus, given a set of four UCB angular fluxes for a rectangular cell, both interpretations of the UCB unknowns produce the same value of the cell-averaged angular flux. However, in problems that have fixed sources, the interpretation does affect cell-averaged solutions, as we discuss and demonstrate below.

In any transport spatial discretization the $\sigma_t\psi$ and Q terms must be treated consistently: the two quantities in a given discrete equation must represent values at the same spatial point or values resulting from the same spatial integration. It follows that in problems with fixed sources, including our MMS problems, one must choose an interpretation for the UCB unknowns and define the associated Q_c values accordingly. In what follows we explore the accuracy of the UCB methods for our MMS problems for both the vertex and corner-averaged interpretation of their unknowns.

For our exploration we will need three different kinds of Q values. In all cases we begin by projecting the MMS source onto bilinear basis functions in each cell, producing a function that we call Q^{BL}_{MMS}. Then for UBLD, the value that appears in the i-th equation is a weighted integral:

$$Q_i^{mom} = \int_V Q^{BL}_{MMS}(x,y)b_i(x,y)\,dV \tag{17}$$

We shall call this the "moment" value. For FLBLD, and for the vertex-centered interpretation of UCB unknowns, the value that appears in the i-th equation is the value at the i-th vertex:

$$Q_i^{vert} = Q^{BL}_{MMS}(x_i,y_i) \tag{18}$$

We shall call this the "vertex" value. For the corner-averaged interpretation of UCB unknowns, the value that appears in the i-th equation is the average over the i-th corner subcell:

$$Q_i^{avg} = \int_{V_i} Q^{BL}_{MMS}(x,y)\,dV \tag{19}$$

The UBLD and FLBLD methods should be exact for the bilinear MMS problem, because the solution resides in the space spanned by their basis functions. We have verified this for our implementation, as Table I shows. Table I also shows the errors that are introduced by using the "wrong" source values (moment values in FLBLD and vertex in UBLD).

Q values used	UBLD	FLBLD
Moment	0	0.0076
Vertex	0.012	0

TABLE I. E_A for bilinear MMS problem for DFEM spatial discretizations with different source values.

Table II provides results from the two UCB methods for the bilinear MMS problem. For this problem, the "vertex" and "average" interpretations of the UCB97 unknowns lead to similar errors, but the "average" interpretation of the UCB05 unknowns produces a more accurate result than does the "vertex" value. We shall keep this in mind as we continue the exploration of MMS problems.

Q values used	UCB97	UCB05
Average	0.058	0.016
Vertex	0.050	0.140

TABLE II. E_A for bilinear MMS problem for UCB spatial discretizations with different source interpretations.

4. MMS for Order of Convergence

We consider a second set of MMS problems with solutions of the form:

$$\psi(x,y,\vec{\Omega}) = 10 + 5\sin\left(\frac{\pi x}{3}\right)\sin\left(\frac{\pi y}{3}\right), \tag{20}$$

for $x \in [0,3]$, $y \in [0,3]$ and $\vec{\Omega} = \langle 0.3500212,\ 0.8688903\rangle$. The problems have no scattering. We can vary σ_t to study optically thin, thick, and intermediate problems. Here we present results with $\sigma_t = 1$ and $\sigma_t = 10^6$, with $\Delta x = \Delta y$. We vary the number is cells along each axis, $N_{z,x} = N_{z,y}$, and study solution convergence in the E_A metric as the number of cells varies from 1×1 to 1024×1024. We observe the behavior of the UCB methods with both the "vertex" and "average" interpretations of their unknowns.

Recall that UCB methods were designed to mimic FLBLD in problems with optically thick cells in which the total source dominates the streaming term. Let us consider an optically thick problem, with $\sigma_t = 10^6$, and let us adopt the interpretation that UCB unknowns are vertex values, like the FLBLD unknowns. The results are shown in Fig. 12. We observe that for the coarsest meshes in this optically thick problem, both UCB methods provide essentially the same solutions as both DFEMs. These nearly identical solutions exhibit the second-order convergence in this mesh-resolution range. This is as expected, given that the UCB methods were designed for this optically thick, total-source-dominated limit. For the two most highly refined meshes (512×512 and 1024×1024), the two UCB methods become noticeably less accurate than the two DFEMs, and UCB05 becomes slightly less accurate than UCB97.

We consider next the same optically thick problem but choose the interpretation that UCB unknowns are spatial averages over corner subcells. The results are provided in Fig. 13,

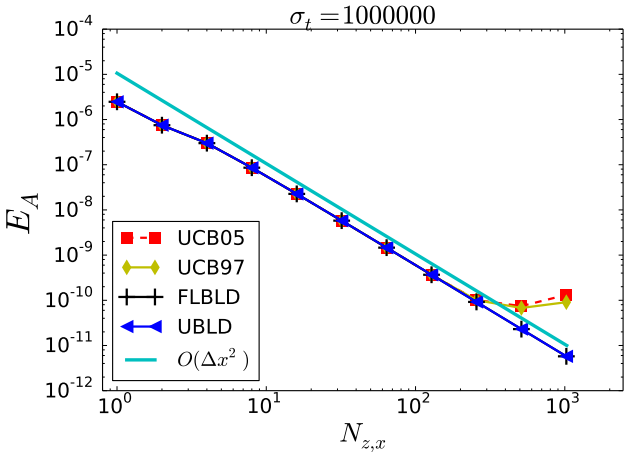

Fig. 12. Convergence of E_A for smooth MMS problem with $\sigma_t = 10^6$, interpreting UCB unknowns as vertex values. All four methods produce essentially identical results except for the two most refined meshes, where the UCB methods become less accurate.

with the DFEM results repeated for easy reference. The difference from the "vertex" interpretation is dramatic. UCB97 and UCB05 produce roughly identical results, but under the "average" interpretation these results are substantially worse than they were under the "vertex" interpretation. We see that, at least with optically spatial cells with strong total sources, UCB unknowns are best interpreted as vertex values. In this kind of problem, interpreting UCB unknowns as corner-averaged values leads to terribly inaccurate solutions.

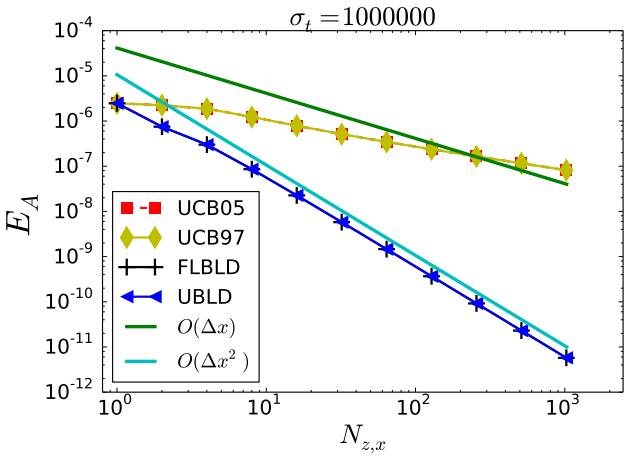

Fig. 13. Convergence of E_A for smooth MMS problem with $\sigma_t = 10^6$, interpreting UCB unknowns as spatial averages over corner subcells. The two DFEM solutions are indistinguishable and the two UCB solutions are indistinguishable.

We turn next to problems with spatial cells with intermediate and small optical thickness, which we obtain by setting $\sigma_t = 1$. Fig. 14 presents E_A as function of the number of zones in the x direction for the four methods studied here, interpreting the UCB unknowns as vertex values. We observe that in this problem: the UBLD E_A is proportional to Δx^3, the FLBLD and UCB97 E_A values are proportional to Δx^2, the UCB05 E_A values are relatively large and proportional to Δx, and the UCB97 solution closely approximates the FLBLD solution. We see that in this smooth test problem, UCB97 achieves in the thin-cell limit the goal that it achieved in the thick-cell limit, namely that it achieves a good approximation of the FLBLD solution. The first-order convergence of UCB05 is consistent with the behavior observed in the ray-propagation problem.

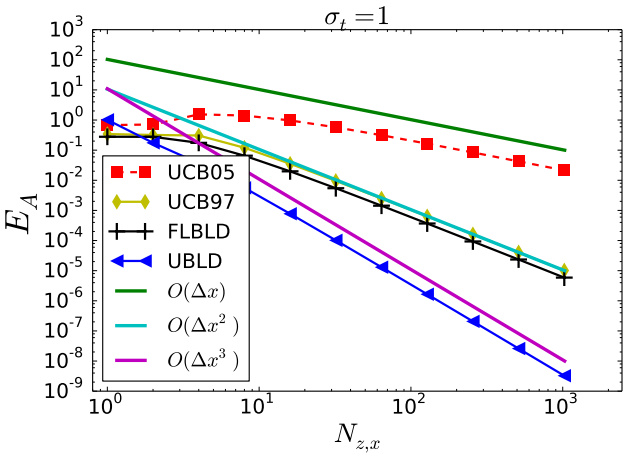

Fig. 14. Convergence of E_A for smooth MMS problem with $\sigma_t = 1$, interpreting the UCB unknowns as vertex values. The UCB97 curve is partially hidden by the second-order trendline.

We reconsider the $\sigma_t = 1$ problem under the interpretation that UCB unknowns are spatial averages over corner subcells. Fig. 15 presents the results, with the DFEM results repeated for easy reference. We observe that in this problem the UCB05 E_A values are an order of magnitude smaller than they were under the "vertex" interpretation, but they remain proportional to Δx. The UCB97 results are not substantially different than they were under the "vertex" interpretation.

IV. CONCLUSIONS

Corner-balance (CB) methods were originally developed to extend the performance of rectangle-cell FLBLD to arbitrary polygonal cells, especially for problems with optically thick, diffusive spatial cells. The first step in CB development was the recognition that each FLBLD unknown satisfies a conservation equation on a "corner" subcell. In this conservation equation, the FLBLD vertex-centered unknown also plays the role of the corner-averaged flux, and the fluxes on intra-zone corner surfaces are simple averages of the neighboring vertex values. The "Simple" corner balance (SCB) method generalized this directly to polygonal cells, and the "Upstream" corner balance (UCB) methods have attempted to obtain approximately the same solutions without inverting the within-cell matrices that DFEMs or SCB require.

UCB97 and UCB05 are two examples of upstream cor-

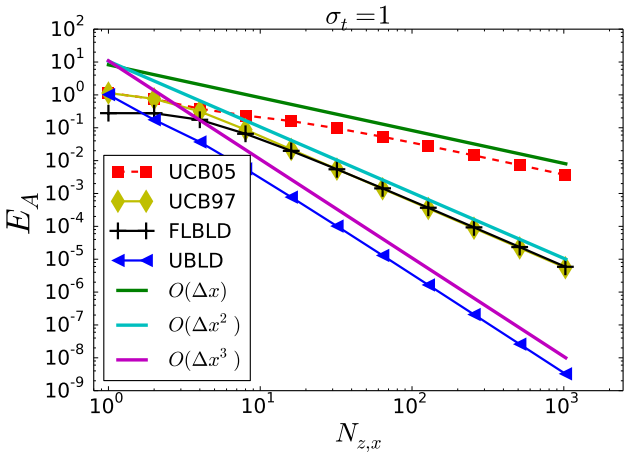

Fig. 15. Convergence of E_A for smooth MMS problem with $\sigma_t = 1$.

ner balance spatial discretizations. UCB97 has an implicit requirement that the difference between the "corner" angular flux and any incident angular fluxes on the immediately adjacent zone surfaces tend to zero as spatial zones are refined. This is because it multiplies this flux differences by a coefficient that becomes unbounded for optically thin cells. In multi-dimensional calculations, this condition is not always satisfied. UCB97 can exhibit instability, with oscillations that grow in magnitude, as the spatial mesh is refined in problems without smooth solutions, as we have illustrated using a ray-propagation problem. UCB05 is equivalent to UCB97 in slab geometry, but it relates outgoing, incoming, and corner-averaged fluxes using an equation whose coefficients are well behaved. UCB05 remains stable as the spatial mesh is refined even in the presence of zones with high aspect ratios, but this comes at the cost of increased numerical diffusion and a reduced order of accuracy for smooth problems.

We have demonstrated that in problems with optically thick spatial cells and strong total sources, both UCB97 and UCB05 do obtain the FLBLD solution, as they were designed to do. This is true only if the "corner" unknowns are interpreted as vertex values, as they are in FLBLD.

Our test problems also indicate that if cells are not sufficiently thick, the UCB results can become less accurate than the FLBLD results. On the finest meshes for problems with smooth solutions, UCB97 again reproduces very nearly the FLBLD results, but UCB05 is significantly less accurate.

In summary, each UCB methods studied here has a flaw for some class of problems. Both methods perform well in the thick diffusion limit. UCB97 performs well for most problems but can produce unacceptable oscillations in some fine-mesh problems with solutions that lack smoothness. UCB05 resists oscillations but is only first-order accurate and exhibits significant numerical diffusion.

When the CB methods were originally developed there were at most a few options for obtaining FLBLD-quality solutions on polygonal cells. Since that time the PieceWise Linear Discontinuous (PWLD) method has been developed to fill this gap [9, 10, 11, 12]. PWLD has been shown to maintain the thick diffusion limit and to converge angular flux errors second order in space in both the optically thick and thin limits. But, PWLD requires the inversion of an $N \times N$ matrix to calculate the angular fluxes on an N-vertex polygon, whereas UCB methods obtain their solutions by marching across the polygon one corner at a time and thus may be computationally faster. In light of the results present here, however, for some classes of problems the solid performance of a DFEM such as PWLD may be worth its additional cost relative to UCB. Further, the computational performance of PWLD implementations has yet to be studied fully and optimized, and as we move towards more advanced, heterogeneous computing architectures, the additional cost of the matrix inversion may be diminishingly small when compared with sweeping the corners of a spatial zone.

V. ACKNOWLEDGMENTS

This work was performed under the auspices of the U.S. Department of Energy by Lawrence Livermore National Laboratory under contract DE-AC52-07NA27344. We thank Teresa S. Bailey for many helpful discussions and for encouraging this effort.

REFERENCES

1. M. L. ADAMS, "Subcell Balance Methods for Radiative Transfer on Arbitrary Grids," *Transport Theory and Statistical Physics*, **26**, *4 &5*, 385–431 (1997).
2. K. THOMPSON, "Private communication," (Jan. 2017).
3. K. A. MATHEWS, "On the Propagation of Rays in Discrete Ordinates," *Nuclear Science and Engineering*, **132**, 155–180 (1999).
4. C. LINGUS, "Analytical Tests Cases for Neutrons and Radiation Transport Codes," in "Second Conference on Transport Theory," United States Atomic Energy Commision- Division of Technical Information, Los Alamos, New Mexico (January 1971), pp. 655–659.
5. M. L. ADAMS, "A New Transport Discretization Scheme for Arbitrary Spatial Meshes in XY Geometry," in "Proceedings of the American Nuclear Society International Topical Meeting on Mathematics and Computation," Available as LLNL Tech. Report UCRL-JC-105974 (April 1991).
6. E. W. LARSEN and J. E. MOREL, "Asymptotic Solutions of Numerical Transport Problems in Optically Thick, Diffusive Regimes II," *Journal of Computational Physics*, **83**, 212–236 (1989).
7. M. L. ADAMS, "Discontinuous Finite Element Transport Solutions in Thick Diffusive Problems," *Nuclear Science and Engineering*, **137**, 298–333 (2001).
8. M. L. ADAMS and P. F. NOWAK, "Asymptotic Analysis of a Computational Method for Time- and Frequency-Dependent Radiative Transfer," *Journal of Computational Physics*, **46**, 366–403 (1998).
9. H. G. STONE and M. L. ADAMS, "A Piecewise Linear Finite Element Basis with Application to Particle Transport," in "Proceedings of the ANS Topical Meeting Nuclear Mathematical and Computational Sciences," Gatlinburg,

TN (April 6-11 2003).

10. T. S. BAILEY, *The Piecewise Linear Discontinuous Finite Element Method Applied to the RZ and XYZ Transport Equations*, Ph.D. thesis, Texas A&M University (May 2008).
11. T. S. BAILEY, M. L. ADAMS, J. H. CHANG, and J. S. WARSA, "A Piecwise Linear Discontinuous Finite Element Spatial Discretization of the Transport Equation in 2D Cylindrical Geometry," in "Proceedings of International Conference on Mathematics, Computational Methods, and Reactor Physics," Saratoga Springs, New York (May 2009).
12. T. S. BAILEY, W. D. HAWKINS, and M. L. ADAMS, "A Piecewise Linear Discontinuous Finite Element Spatial Discretization of the S_N Transport Equation for Polyhedral Grids in 3D Cartesian Geometry," in "The 22^{nd} International Conference on Transport Theory," Portland, OR, USA (September 2011).